OPEN ACCESS

Multi-Week Cycling of a Nonaqueous Flow Battery Using Tris-Bipyridine Iron (II) Triflate without Additional Supporting Electrolyte

Journal of The Electrochemical Society, 2023 **170** 060510

Multi-Week Cycling of a Nonaqueous Flow Battery Using Tris-Bipyridine Iron (II) Triflate without Additional Supporting Electrolyte

Kirk P. Smith,[1,2] Rohit Rungta,[1] Andrew A. Wang,[1,2] and Charles W. Monroe[1,2,z]

[1]*Department of Engineering Science, University of Oxford, Oxford, OX1 3PJ, United Kingdom*
[2]*The Faraday Institution, Harwell Campus, Didcot, OX11 0RA, United Kingdom*

Tris-bipyridine iron (II) triflate was synthesized and used as an active species to demonstrate a symmetric disproportionation redox-flow-battery chemistry that works without a supporting electrolyte. Solutions of this coordination complex salt (0.1 M in acetonitrile), in which the cation provides the redox activity, were qualitatively characterized with cyclic voltammetry and used to perform extended full-cell charge/discharge cycling and impedance testing in reactors containing a porous Daramic 175 separator membrane. The cell, based on 10 ml reservoirs of active liquid, survived for more than eight hundred cycles, with charge/discharge cycling taking place over a period of more than two weeks. Four cycling protocols were evaluated to investigate the effects of applied current and depth-of-discharge on cell performance. The system allows for hundreds of cycles above 50% state-of-charge and is capable of exceeding 80% round-trip energy efficiency.
 [DOI: 10.1149/1945-7111/acd873]

Manuscript submitted December 28, 2022; revised manuscript received April 22, 2023. Published June 6, 2023. *This paper is part of the JES Focus Issue on Frontiers of Chemical/Molecular Engineering in Electrochemical Energy Technologies in Honor of Robert Savinell.*

Recently Fisher (née Laramie) et al. identified several possible advantages of flow-battery chemistries that do not require additional supporting electrolytes. These systems, known as "common ion" or "rocking chair" configurations (as opposed to "salt splitting" configurations that involve two or more passive supporting ions), use solutions of ionic active species which are complemented by a single, non-redox-active counterion, which ideally carries all charge through the separator to main electroneutrality as the battery's state of charge swings.[1] Implementations of common-ion redox flow batteries can be achieved in two ways: they can either incorporate a single active salt with a redox-inactive ion and a counterion that can electrochemically disproportionate;[2,3] or two active salts can be used, which share a common electrochemically inert ion but have different redox-active counterions.[1,4] Both common-ion approaches can be used to construct symmetric flow batteries, which have identical positive and negative electrolyte compositions in the discharged state.[1–3,5,6] Symmetric flow batteries are crossover tolerant and therefore do not require an ion-exchange membrane, allowing the use of more chemically stable, lower-cost, lower-resistivity, unselective porous separators, which are widely available.

Salts of coordination complex cations involving iron centers with aromatic ligands are a promising set of compounds for formulating common-ion, supporting-salt-free, symmetric flow battery electrolytes. Iron acts as the coordination center and is chelated octahedrally by redox-active aromatic ligands, a popular choice being 2,2'-bipyridine, abbreviated "bpy".[7] Such compounds have been combined with electrochemically stable anions to create batteries with discharge potentials above 2 V.[3,5,6,8]

In this work we study coordination complex salts based on tris-bipyridine iron (II), or $Fe(bpy)_3^{2+}$. The iron center of this complex cation offers the Fe^{2+}/Fe^{3+} oxidative couple and its ligand is also redox-active, providing a reductive couple that enables the cationic complex to disproportionate electrochemically.[9]

The three bidentate bpy ligands push the potential of the metal-centered Fe^{2+}/Fe^{3+} reaction in the oxidizing direction, from 0.8 V to 1.0 V vs the standard hydrogen electrode (SHE) in aqueous solution.[10] A significant electrochemical feature of the $Fe(bpy)_3^{2+}$ complex cation is that it allows for one or more reversible negative electron-transfer events at −1.3 V vs SHE (converted from measurements in nonaqueous solutions with a ferrocene/ferrocenium internal standard), more negative than conventional iron plating/stripping occurring at −0.45 V vs SHE (converted from measurements in aqueous solution, relative to a saturated calomel electrode).[9–11] Thus, the bpy ligands widen the cell potential achievable with an iron-centered complex at both ends.

Given an appropriate redox-active cation like $Fe(bpy)_3^{2+}$, electrochemically stable anions, such as perchlorate (ClO_4^-) or tetrafluoroborate (BF_4^-),[6,8] can be used to provide charge neutrality to the complex salt, as well as providing the functionality of a supporting electrolyte when the active salt is dissolved in solution for the purpose of operating a flow battery. This multifunctional nature of the complex-salt active species could offer a pathway to cost savings and simpler formulation; Darling et al. have demonstrated that supporting electrolytes are a major cost driver in nonaqueous flow-battery systems.[12] Fisher et al. and Milshtein et al. discuss more granularly the technoeconomic opportunities of flow-battery systems without additional supporting electrolyte.[1,2] A symmetric, crossover-tolerant, high-voltage, supporting-salt-free, iron/organic-based flow battery electrolyte would be desirable, and many researchers have advanced the field toward the possibility of this one-solute, one-solvent formulation.

The tris-bipyridine iron (II) cation, $Fe(bpy)_3^{2+}$, has been studied electrochemically in nonaqueous solutions for more than half a century. Ward claimed the first nonaqueous study of the Fe^{2+}/Fe^{3+} couple of the ClO_4^- salt in acetonitrile[13] in 1958. Ward studied the positive couple of $Fe(bpy)_3^{2+}$, but not the ligand reductions. Herzog and Taube wrote the original paper on the stabilization of low-oxidation state transition-metal centers by 2,2'-bipyridine,[14] which Hall and Reynolds followed by preparing and characterizing the $Fe(bpy)_3^{2+}$ compound with reduced ligands.[15] By the end of the 1960s, Tanaka and Sata had studied the reduction processes of $Fe(bpy)_3^{2+}$ in nonaqueous solution with voltammetry.[9] Singh identified the potential of $Fe(bpy)_3^{2+}$ for battery applications in 1984,[16] and in 1988 the Matsumura-Inoue group studied the metal-centered positive and ligand-centered negative charge-transfer processes of Ru and Fe 2,2'-bipyridine complexes with voltammetry[17] and built a redox flow battery based on tris-bipyridine ruthenium(II) tetrafluoroborate.[18] This latter paper seems to report both the first nonaqueous flow-battery chemistry and the first attempt to explore

[z]E-mail: charles.monroe@eng.ox.ac.uk

the reduced ligand-centered 2,2'-bipyridine couple for reversible bulk electrolysis. The team noted that system behavior depends on membrane type, observed performance improvement with higher electrolyte flowrates, and discussed possible instability of the reduced complex. They found that substituting the bidentate acetylacetonate ligand for 2,2'-bipyridine improved stability, suggesting why future nonaqueous flow battery researchers may have focused more on acetylacetonate compounds.

Since 2000, researchers have been wary of the reduced $Fe(bpy)_3^{2+}$ complex. Chakrabarti et al. observed poor performance for the ClO_4^- salt in acetonitrile.[8] Mun et al. from Samsung used $Fe(bpy)_3^{2+}$ in a flow battery, but only for the positive couple, using a nickel congener, $Ni(bpy)_3^{2+}$, for the negative couple that underwent reversible reduction at a less negative potential than the ligands of the iron complex.[19] An overlapping group of Samsung researchers, Park et al. were granted a US patent in 2010[20] on an entire class of transition-metal complexes with aromatic ligands for use in symmetric flow batteries, including $Fe(bpy)_3^{2+}$. Later, Mun et al. cycled both the $Fe(bpy)_3^{2+}$ compound's negative and positive redox couples using bis(trifluoromethanesulfonyl)imide (TFSI) as the anion for 8 cycles at 0.8 mA cm^{-2} while using tetraethylammonium tetrafluoroborate ($TEABF_4$) as additional supporting electrolyte.[5] By 2021, Cammack et al. had furthered cycling of the BF_4^- salt of $Fe(bpy)_3^{2+}$ to 20 cycles at 2.0 mA cm^{-2}, while separately using additional supporting electrolytes of $TEABF_4$, tetrabutylammonium tetrafluoroborate ($TBABF_4$), and tetrabutylammonium bis(trifluoromethanesulfonyl)amide (TEATFSI).[6]

Fisher et al. observed rapid capacity fade of the BF_4^- salt of $Fe(bpy)_3^{2+}$ in bulk electrolysis experiments, and used the compound for positive half-reaction in a flow cell with ferrocenylmethyl dimethyl ethyl ammonium tetrafluoroborate (Fc1N112-BF_4) to supply the negative couple and $TEABF_4$ as supporting electrolyte.[1] The same team saw less rapid fade during bulk electrolysis when using tridentate terpyridine ligands instead of bipyridine.[4] Fisher hypothesized that ligand dissociation could be involved in the performance decay. Additionally, BF_4^- has been observed by Silcox to interfere with the performance of nonaqueous flow batteries using organic active species.[21] Notably, Cammack et al. specifically attributed instability to the BF_4^- anion when working with $[Fe(bpy)_3](BF_4)_2$.[6]

Milshtein et al. further investigated the $Fe(bpy)_3(BF_4)_2$ system, but flow-cell studies again only used $Fe(bpy)_3^{2+}$ for the positive couple. Nevertheless, they successfully cycled the cell using Fc1N112-BF_4 to supply the negative couple without supporting electrolyte in a common-ion configuration.[2] The MacFarlane group have also explored $Fe(bpy)_3^{2+}$ for the purpose of achieving such a flow battery, studying the electrochemistry[11] and mixed ligand complexes,[22] with Blesch thoroughly investigating the complex and cycling its bis(fluorosulfonyl)imide (FSI) salt in a recent thesis.[3] Blesch, it appears, produced the only report cited here in which $Fe(bpy)_3^{2+}$ disproportionation was probed without additional supporting electrolyte.

In summary, the overlapping relations and attributes of previously explored electrolyte compositions are presented diagrammatically in Fig. 1. The figure also indicates the definitions of terms used in this paper to describe flow-battery chemistries.

Redox-active species capable of disproportionation are also described as "bipolar"; Chen has recently categorized bipolar species into five types.[25] In that classification scheme, a coordination compound like $V(acac)_3$, which accesses three oxidation states with one redox center, would be Type I. A cationic coordination complex like $Fe(bpy)_3^{2+}$ can access at least three oxidation states, but the Fe II/III reaction is understood to be metal-centered, while the reduction reactions are ligand-centered.[26] Due to the presence of multiple redox centers in the cationic complex (metal center and redox-active ligands), $Fe(bpy)_3^{2+}$ could be considered as Type II ("at least two different redox centers in the same molecule") or Type III ("materials with different redox units connected directly") within Chen's taxonomy.

For the present study, the triflate anion ($CF_3SO_3^-$) was used as the counteranion for the $Fe(bpy)_3^{2+}$ cation, with the aim of achieving more stable cycling performance than salts with BF_4^- and FSI^-, while avoiding the known tendency of BF_4^- to hydrolyze.[27,28] Researchers at the University of Ferrara used the triflate salt of $Fe(bpy)_3^{2+}$ as a posolyte for asymmetric common-ion cells with the cobalt congener as negolyte,[23,24] but $[Fe(bpy)_3](CF_3SO_3)_2$ remains untested in a symmetric configuration. Note that triflate is a sound choice for engineering purposes because of the availability of pure anhydrous triflic acid, and provides a simple variation on the chemical characteristics of TFSI.

Methods

Acetonitrile (HPLC grade, Fisher, UK) and diethyl ether (puriss, Honeywell, Germany) were sparged with argon and dried over 4 Å molecular sieves (Sigma-Aldrich, USA). After sparging, acetonitrile was dispensed over an activated alumina column with a solvent purification system (Inert PureSolv, USA) before storage over molecular sieves. Both solvents were confirmed anhydrous using Karl Fischer coulometry. All experiments were conducted in an argon-filled glove box with <1.0 ppm O_2 and H_2O (PureLab, Inert Technologies, USA), and all electrochemical measurements were performed with an Ivium Octostat.

Synthesis.—Synthesis of the $CF_3SO_3^-$ salt of $[Fe(bpy)_3]^{2+}$ started by following the procedure of Hagen.[29] About 5% (mole basis) excess iron powder was added to a mixture of acetonitrile and triflic acid under heating and stirring. Hydrogen gas was evolved during this process. After the reaction subsided, the excess iron was filtered off over a Celite pad, and the supernatant concentrated by vacuum. This yielded the acetonitrile-ligated iron (II) triflate salt. Similar to Hagen's observations,[29] varying degrees of ligation by acetonitrile were observed depending on the extent of drying, with a pale off-white free-flowing powder seeming to correspond to $Fe(CF_3SO_3)_2.2ACN$, and a minty green wet-looking salt seeming to correspond to $Fe(CF_3SO_3)_2.4ACN$. When observed, orange compound in the salt, likely Fe^{3+}, was removed by washing with diethyl ether or acetonitrile. In an argon-filled glove box, the $Fe(CF_3SO_3)_2.2ACN$ was then reacted with a slight (5%–10% mole basis) excess of colorless 2,2'-bipyridine stock solutions as done by Park et al.,[20] immediately producing the distinctive dark red/purple color of the $Fe(bpy)_3^{2+}$ cation. This mixture was stirred for a few hours before drying under vacuum and washing thoroughly with diethyl ether (to remove excess 2,2-bipyridine), and again drying under vacuum on a Schlenk line.

Voltammetry.—All voltammetry experiments used a 3 mm glassy-carbon disc working electrode (BASi) and coiled Pt-wire counter electrode. The reference electrode was a nonaqueous silver/silver nitrate kit (BASi) using a silver wire and a filling solution of 0.01 M silver nitrate and 0.1 tetraethylammonium perchlorate in acetonitrile, separated from bulk solution with a frit, as commonly used for acetonitrile-based electrolyte studies.[30]

In addition to cyclic voltammetry, the technique of differential pulse voltammetry (DPV) was used to observe the voltammetric behavior of the $[Fe(bpy)_3](CF_3SO_3)_2$ complex in an attempt to more clearly resolve the ligand reduction processes. DPV superimposes an alternating current waveform on top of a linear-sweep voltammogram. This process seeks to improve the detection of the relevant Faradaic component of the voltammogram relative to the capacitive component.[31] DPV was recorded at 100 mV s^{-1} starting from +1 V with a voltage step of 3 mV, pulse amplitude of 10 mV, and pulse time of 10 ms (the standard settings in the IviumSoft potentiostat control software).

Flow cell cycling and impedance testing.—An identical flow-cell configuration was used as in our previous work,[32] with the following adjustments. Instead of glass vials, perfluoroalkoxy alkane

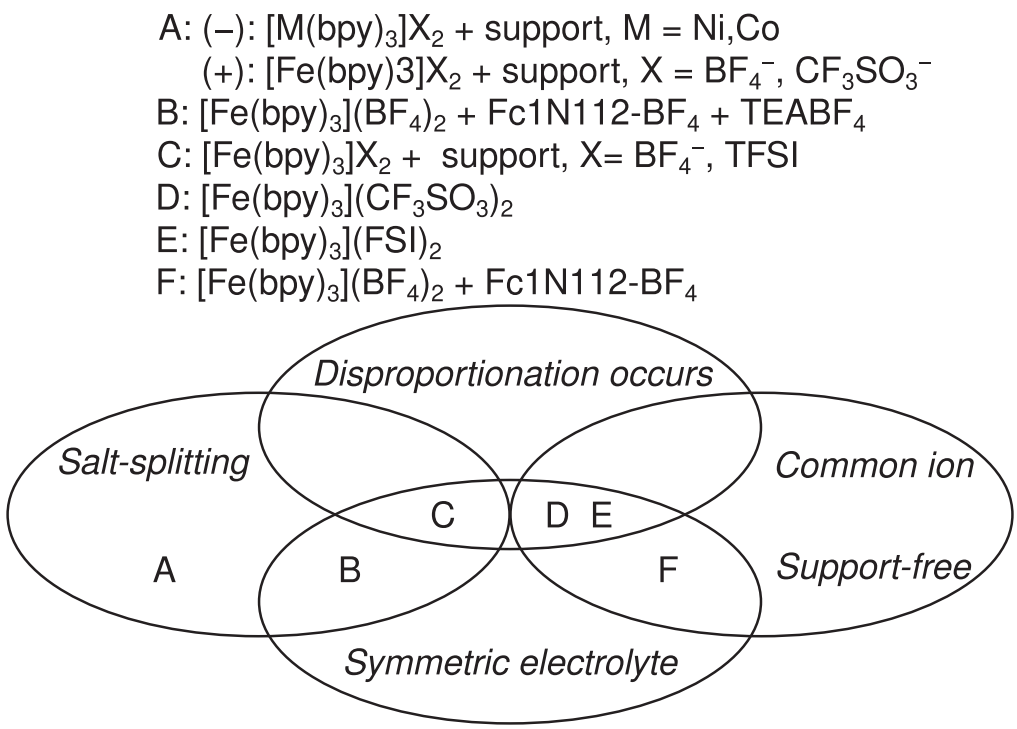

Figure 1. Venn diagram showing the commonalities and differences among cited electrolyte compositions for redox flow batteries in terms of the attributes of disproportionation, symmetric electrolyte, salt-splitting, and common ion/support-free operation. References are A: Mun et al. (2012),[19] Meda et al. (2018),[23] Benazzi et al. (2018),[24] B: Laramie et al. (2016),[1] C: Cammack et al. 2021,[6] Mun et al. (2018),[5] D: this work, E: Blesch (2022),[3] and F: Milshtein et al. (2017).[2]

(PFA) sealed jars (10 ml, Savillex) were used so free headspace in the system was minimized and electrolyte volume imbalance would be passively mitigated. Instead of Celgard 4560, Daramic 175 was used as the separator.

The electrolyte used for charge/discharge cycling was 20 ml (total) 0.1 M $[Fe(bpy)_3](CF_3SO_3)_2$ in acetonitrile, which was apportioned equally between electrolyte reservoirs at the outset of experiments. Constant-current cycling was performed at both ± 20 mA cm^{-2} and at ± 10 mA cm^{-2} to different maximum states of charge.

Voltammetry suggests that the nominal cell potential provided by the $[Fe(bpy)_3](CF_3SO_3)_2$ chemistry should be ~2.4 V. In order to put the same amount of charge into the cell with each cycle, fixed-period galvanostatic charging steps were attempted. As a secondary charge-termination condition, a high-voltage cutoff of 3.5 V was chosen to maintain safe operation while accommodating increases in overpotential during cycling. All cycles included a 20 second open-circuit hold after the charge step. Then, a constant-current discharge at the same current density used for charging was applied until cell voltage dropped below 1.4 V.

Four cycling protocols, designated **I**, **II**, **III**, and **IV**, were applied to the same cell and electrolyte. Protocol **I** applied a current density of ± 20 mA cm^{-2} with a 439-second charging step, equivalent to 20% theoretical state-of-charge (ignoring self-discharge). After over 500 cycles and 6 days of cycling with Protocol **I**, Protocol **II** was applied, using the same current density and removing the charging step time limit, allowing the cell to hit the 3.5 V charging cutoff. Approximately 20 cycles of Protocol **II** were performed, to let the cell stabilize at its new operating conditions and observe the accessible capacity. Next, Protocol **III** was applied, also at ± 20 mA cm^{-2}, with a fixed-duration charge cutoff of 1140 seconds, equivalent to 52% of the theoretical maximum state-of-charge (ignoring self-discharge). After 175 cycles of Protocol **III**, Protocol **IV** was implemented, which halved the applied current density to ± 10 mA cm^{-2} and a fixed charging time of 2280 s, equivalent to 52% theoretical state-of-charge (ignoring self-discharge).

Constant-voltage electrochemical impedance spectroscopy was performed about the open-circuit voltage after every 10 cycles. Impedance spectra were recorded using a 10 mA current amplitude, with 5 frequencies per decade from 100 mHz to 100 kHz.

All charge/discharge and impedance data collected during cycling are available in a data repository that accompanies this article.[33] For clarity, all of the charge/discharge cycling profiles and impedance spectra gathered have not been presented here.

Results

Voltammetry.—Figure 2 compares a cyclic voltammogram of 0.01 M $[Fe(bpy)_3](CF_3SO_3)_2$ in 0.25 M $TEABF_4$ with a voltammogram of 0.01 M $V(acac)_3$ in 0.3 M tetraethylammonium tetrafluoroborate supporting electrolyte under the same test conditions. Figure 3 shows differential pulse voltammograms collected from the same samples as in Fig. 2.

Charge/Discharge cycling.—Figure 4 shows selected charge/discharge profiles across the four different cycling protocols described in the Methods section. The same data is represented in Fig. 5, which shows the efficiencies of the cell across all four cycling protocols along with the cumulative time. Utilization efficiency is defined as the accessed capacity on discharge as a fraction of the theoretical maximum capacity of the electrolyte, on a coulombic basis—equivalent to the state-of-charge range accessed on the discharge step.

Table I presents the mean values and standard deviations of efficiencies shown in Fig. 5 across the four cycling protocols and number of cycles in each and compares them to previous reports.

The flow cell made from 20 ml of 0.1 M $[Fe(bpy)_3](CF_3SO_3)_2$ in acetonitrile cycled for a total of 897 cycles over 18 days. Cycling began at 20 mV cm^{-2} to a conservative 20% state-of-charge (cycling Protocol **I**) for the first 560 cycles, as shown in the top left of Fig. 4. Examining the profiles alongside the cycle-by-cycle efficiencies shown in Fig. 5, one can see that the first ~80 cycles show gradual increases in coulombic and utilization efficiencies, with corresponding decreases in voltaic and energy efficiencies. Then, these

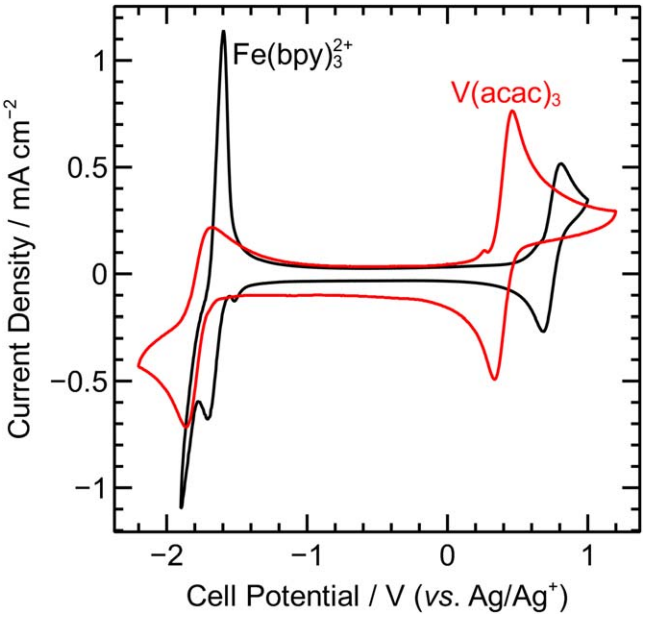

Figure 2. Cyclic voltammograms of 0.01 M V(acac)$_3$, 0.3 M TEABF$_4$ (red) and 0.01 M [Fe(bpy)$_3$](CF$_3$SO$_3$)$_2$, 0.25 M TEABF$_4$ (black) at a scanrate of 100 mV s^{-1} in acetonitrile on a glassy carbon working electrode at 25 °C.

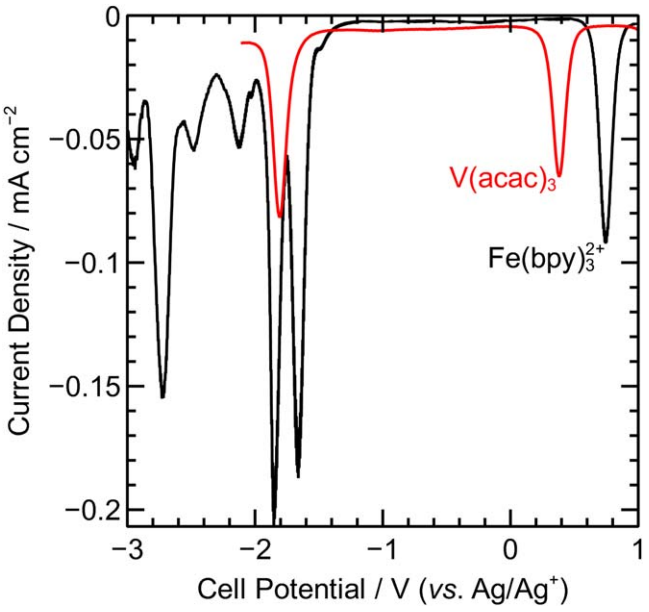

Figure 3. Differential pulse voltammograms of 0.01 M V(acac)$_3$, 0.3 M TEABF$_4$ (red) and 0.01 M [Fe(bpy)$_3$](CF$_3$SO$_3$)$_2$, 0.25 M TEABF$_4$ (black) in acetonitrile on a glassy carbon working electrode at 25 °C The scan of [Fe(bpy)$_3$](CF$_3$SO$_3$)$_2$ shows signatures from the iron II/III positive couple, as well as six sequential reductions of ligated 2,2'-bipyridine ligands to their radical anions, and possibly dianions. For both samples, the scanrate was 100 mV s^{-1} starting from 1 V and progressing in the cathodic direction.

changes accelerate, with couloumbic efficiency quickly climbing to near unity, utilization efficiency plateauing, and voltaic and energy efficiencies approaching a constant decay with both cycle number and time by day three of cycling. System behavior continues without significant change until approximately cycle 350, when the voltaic and energy efficiencies begin decreasing more slowly, plateau, and then start increasing until cycle 560. During this period, the charge/discharge profiles for cycling Protocol **I** shown in the top-left of Fig. 4 show the following features. Cycle time increases due to increased discharge duration as the coulombic efficiencies increase.

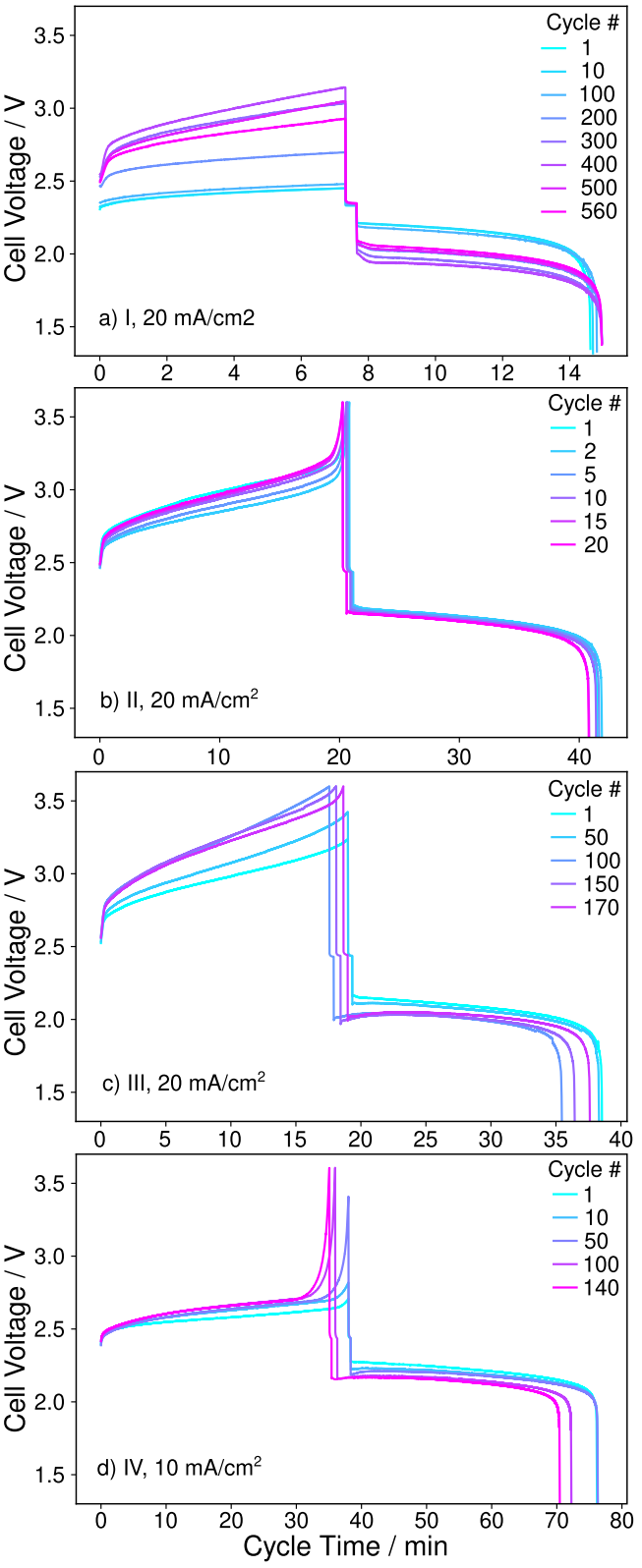

Figure 4. Selected charge/discharge profiles of a [Fe(bpy)$_3$](CF$_3$SO$_3$)$_2$ flow cell undergoing charge/discharging cycling under chronologically sequential Protocols **I**, **II**, **III**, and **IV**.

The open-circuit hold between charging and discharging steps relaxes to a constant potential. Overpotential on charge increases more than on discharge, and all overpotentials show the same non-

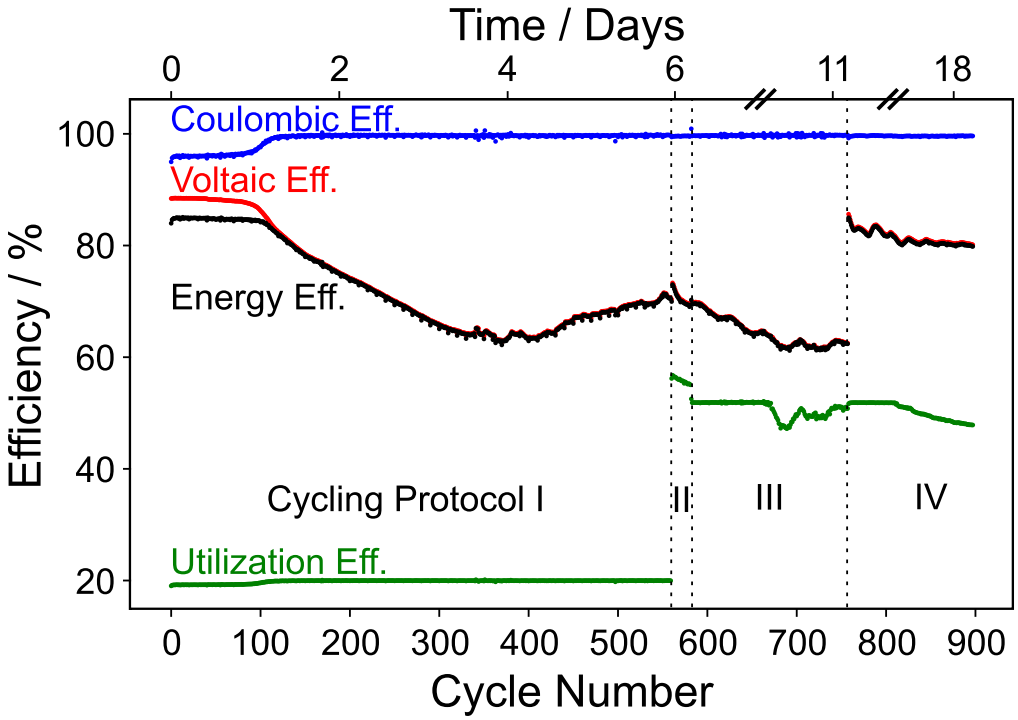

Figure 5. Efficiency data for the $[Fe(bpy)_3](CF_3SO_3)_2$ flow cell.

Table I. Summary of the present and recent efforts to cycle the $Fe(bpy)_3^{2+}$ cation's positive and negative couples simultaneously in a symmetric redox-flow cell. The table shows electrolyte composition, cycle count, current density *j*, coulombic (CE), voltaic (VE), energy (EE) and utilization (UE) efficiencies of the cycled cell(s), along with their standard deviations (for the present work). Abbreviations are bis(trifluoromethanesulfonyl) imide (TFSI), bis(fluorosulfonyl)imide (FSI), tetraethylammonium (TEA), tetreafluoroborate (BF_4), tetrabutylammonium (TBA), propylene carbonate (PC), acetonitrile (ACN). Parameters of the experimental test cells that are not listed may vary across the cited sources.

	Electrolyte Composition	Cycles	j / mA cm^{-2}	CE / %	VE / %	EE / %	UE / %
Mun et al.[5]	0.2 M $[Fe(bpy)_3](TFSI)_2$ 0.5 M $TEABF_4$ in PC	8	0.8	N/A	N/A	N/A	N/A
Cammack et al.[6]	0.2 M $[Fe(bpy)_3](BF_4)_2$ 0.5 M TBATFSI in PC	20	2.0	92	87	80	30
	0.2 M $[Fe(bpy)_3](BF_4)_2$ 0.5 M $TBABF_4$ in PC	20	2.0	97	88	85	50
	0.2 M $[Fe(bpy)_3](BF_4)_2$ 0.5 M $TEABF_4$ in PC	20	2.0	97	88	85	65
Blesch[3]	0.01 M $[Fe(bpy)_3](FSI)_2$, 0.2 M $TBABF_4$ in PC	12	0.54-1.07	90	90	80	20
	0.4 M $[Fe(bpy)_3](FSI)_2$ in PC	5	1.5	84	76	64	15
This work	0.1 M $[Fe(bpy)_3](CF_3SO_3)_2$ in ACN	560	20.0	99.0 ± 1.3	73.2 ± 8.7	72.4 ± 7.7	19.8 ± 0.3
	(same cell used for all cycles)	21	20.0	99.6 ± 0.0	70.7 ± 1.1	70.4 ± 1.1	55.9 ± 0.5
		176	20.0	99.7 ± 0.2	64.5 ± 2.6	64.4 ± 2.6	50.8 ± 1.4
		140	10.0	99.6 ± 0.1	81.5 ± 1.2	81.2 ± 1.2	50.3 ± 1.5

monotonic behavior as the voltaic/energy efficiencies in Fig. 5: they increase first, then plateau, and then decrease.

After the 560 cycles of Protocol **I**, the time limit on charging was removed and the cell was allowed to charge until it reached the 3.5 V charging limit. During these cycles, the cell reached a much higher state-of-charge—nearly 60%. After 21 cycles with this aggressive charge profile, the cycling protocol was changed, and the charge time was adjusted to access a state-of-charge of at most 52%, chosen so that the cell would not reach its high-voltage cutoff. During the 21 cycles of Protocol **II**, overpotential grew slightly on charge (Fig. 4), reflected in decreasing voltaic and energy efficiencies in Fig. 5. During the 170 cycles of Protocol **III**, overpotential grew steadily, eventually reaching the 3.5 V voltage cutoff, which caused cycle lengths, as well as the voltaic, energy, and utilization efficiencies, to decrease.

After Protocol **III**, the current density was halved to 10 mA cm^{-2} in order to reduce overpotentials and observe continued operation of the system. The charge-step duration was concomitantly adjusted to reach a similar state-of-charge as obtained by the previous protocol. Voltaic and energy efficiencies increased accordingly due to reduced ohmic losses. After the first ∼50 cycles of Protocol **IV**, the high-voltage cutoff was reached again, with a sharp increase in cell voltage this time appearing as the vertical asymptote of a Nernstian charging process. Cycling was terminated after 140 cycles as the cell had provided sufficient data to demonstrate the improved performance of $[Fe(bpy)_3](CF_3SO_3)_2$.

Energy capacity fade rates were calculated on a Wh/L basis compared to a given protocol's initial cycle for each of the four cycling protocols. For Protocol **I**, the fade rate was 0.0053 %/cycle or 0.512 %/day; for Protocol **II**, 0.205 %/cycle or 7.18 %/day; for Protocol **III**, 0.0294 %/cycle or 1.13 %/day; and for Protocol **IV**, 0.0759 %/cycle or 1.484 %/day.

Full-cell impedance testing.—Figure 6 shows Nyquist plots of selected full-cell impedance spectra collected across the entire duration of cell cycling. Over the 897 cycles, the cell impedance was observed to grow. The higher-frequency parts of the impedance spectra in Fig. 6 flatten somewhat with cycle count and the lower-

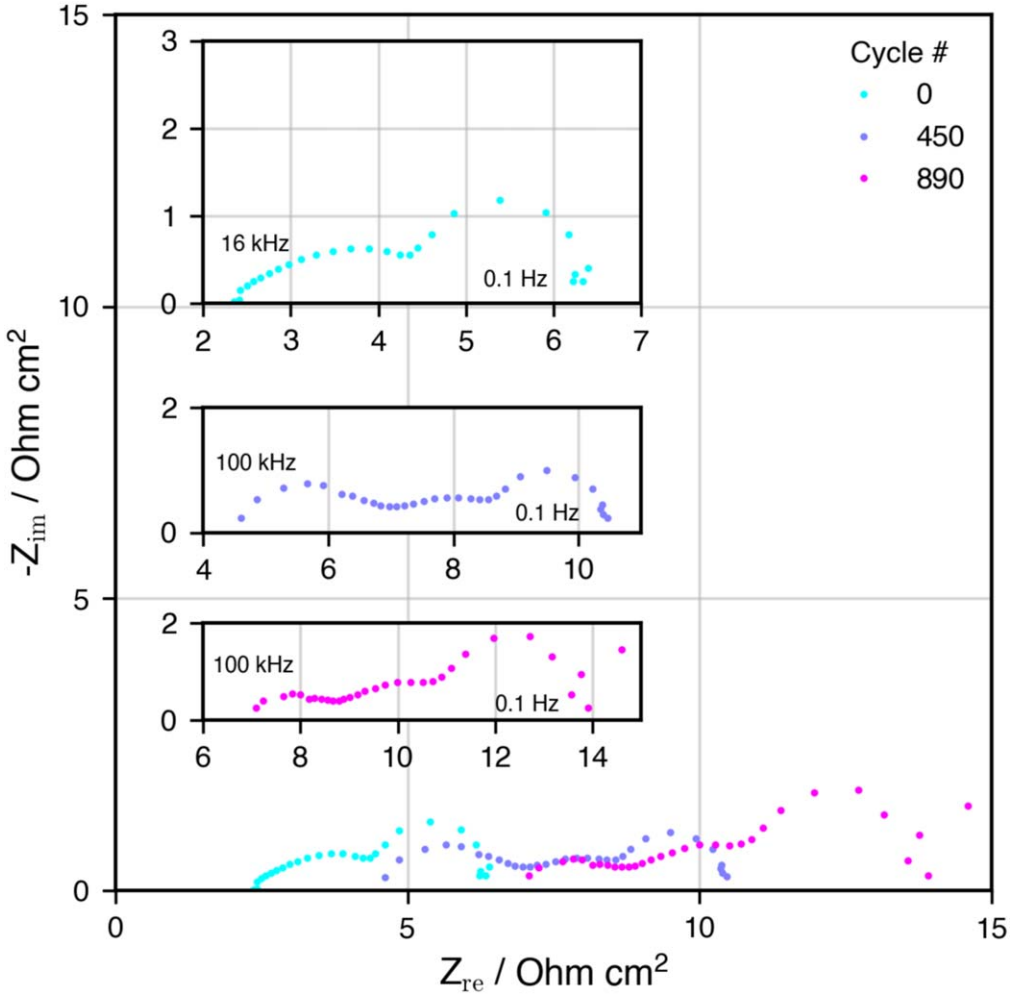

Figure 6. Nyquist plots of impedance spectra collected before cycling, after 450 cycles, and after 890 cycles for the $[Fe(bpy)_3](CF_3SO_3)_2$ flow cell.

frequency regions change qualitatively: the higher-frequency part of the impedance spectrum flattens somewhat with increasing cycle count and the lower-frequency region develops some additional features, including what appears to be a loop at low frequencies.

The most significant observed change in the impedance spectra with cycling was a steady rightward shift of the high-frequency intercepts with the real axis on Fig. 6, which are associated with cell resistance. These resistances, which determine the ohmic losses in the cell, were extracted from impedance data and are presented with respect to cycle number on Fig. 7. Because of the steady increase in cell resistance, Ohmic loss—either by an increase in separator resistance or a decrease in bulk electrolyte conductivity—appears to be the primary culprit that drives the decrease in voltaic and energy efficiencies, as well as the growth of charging and discharging overpotentials seen in Fig. 4.

Although it is not an effect that can be directly visualized in efficiency or impedance data, it should be noted that electrolyte was also observed to accumulate in the negative reservoir over the course of the experiment. The electrolyte also appeared to reduce its total volume over time, presumably due to solvent evaporation. The cell, reservoirs, and associated tubing were sealed as hermetically as possible, but the system has many seals and interfaces through which highly volatile acetonitrile can evaporate into the controlled dry atmosphere of the glovebox.

Discussion

Before probing the electrochemical engineering aspects of this electrolyte formulation, it is worth pointing out some economic

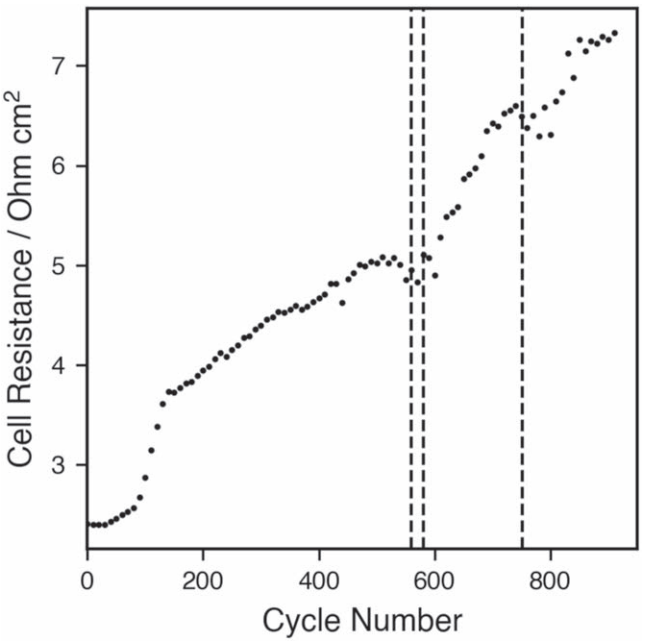

Figure 7. Evolution of the cell resistance, measured from the high-frequency x-intercepts of impedance spectra, during cycling of the $[Fe(bpy)_3](CF_3SO_3)_2$ flow cell. Each dashed vertical line represents a transition between cycling protocols as discussed in the methods section.

concerns. Although cheaper and more readily available than many alternatives, the triflate anion still represents a significant synthetic cost, and efforts to find more affordable and sustainable anions would be useful. Lithium-ion battery electrolyte manufacturers have in 2022 achieved production costs below \$10/kg for 1M $LiPF_6$ in anhydrous propylene carbonate.[34] Darling et al. set an electrolyte cost target for nonaqueous flow batteries of \$5/kg, which appears possible when lithium is eliminated from the formulation in favor of iron—even more so if fluorine could be also eliminated.[12] Their technoeconomic analysis also set targets for the following properties: a cell potential of 3 V, redox-active species molecular weight less than 150 g/mol, active species costs less than \$5/kg and active species solubility over 4 M. For the complex studied here, cell potential is 2.4 V, the bipyridine ligand alone weighs 156 g/mol, and no cycling was performed over 1 M active species concentration, although the solubility limit is higher than the 0.1 M concentration used for the present tests. Improvements on all of these characteristics would be essential for the practical realization of electrolyte designs based on nonaqueous coordinated iron cations.

The cyclic voltammograms of Fig. 2 show how the voltammetric response of $[Fe(bpy)_3](CF_3SO_3)_2$ in neat acetonitrile compares to that of the well-studied $V(acac)_3$ complex with tetraethylammonium tetrafluoroborate supporting electrolyte. The Fe^{2+}/Fe^{3+} couple is more positive than V^{3+}/V^{4+} (0.74 and 0.45 vs Ag/Ag^+, respectively). Ligand reduction of the iron complex is slightly less negative than the V^{3+}/V^{2+} couple (−1.66 and −1.77 vs Ag/Ag^+, respectively), with the potential for the first ligand reduction taken from Fig. 3). The total separation between the redox events of the iron complex is greater than those of vanadium (∼2.4 V vs 2.2 V, respectively), and the clear redox peaks in both voltammograms suggest that electrochemical reversibility of the iron complex compares well to that of $V(acac)_3$. On this basis, kinetic resistance is not expected to be a performance-limiting factor for the iron-based system.

The cyclic voltammograms of Fig. 2 and differential pulse voltammograms of Fig. 3 suggest at least three sequential reduction events for the coordination compound salt. These have been previously been observed for tris(bpy) compounds,[11,19,35] and are logically associated with the three 2,2'-bipyridine ligands of the $Fe(bpy)_3^{2+}$ cation. Note that extreme solvent dependence of charge-transfer processes is common in nonaqueous electrochemistry.[36,37] The behavior observed in other tris(bpy) systems depends on the solvent used, with systems solvated in propylene carbonate showing mass-transfer-limited resolved peaks on the positive scans of the negative couples.

In the differential pulse voltammogram of Fig. 3, the signatures of electron-transfer events are expected to be symmetric about their equilibrium potentials. Because the scan was entirely in the negative direction, the peaks in Fig. 3 have negative currents. A signature of the Fe^{2+}/Fe^{3+} couple appears at 0.7 V vs. Ag/Ag^+. Also, six reduction processes are observed in the negative-potential region. The least negative three occur at similar potentials to those seen in Fig. 2 and other reports, and so seemingly correspond to the stepwise reduction of 2,2'-bipyridine ligands. The most negative three reduction processes also have peak-to-peak separation of ∼150 mV, similar to the least negative three reduction events. These events likely correspond to the formation of dianions of the bpy ligands, behavior that has been observed for different aromatic ligands coordinated to iron in the past.[38]

Most voltammetric studies occur with the bulk solution in the fully discharged state (from a battery perspective) and thus, there may be different behavior of these couples if charge/discharge cycling changes the bulk solution composition. A survey of the literature on tris(bipyridine) reduction processes revealed a debate over where the electrons are stored on the reduced complex—on individual ligands, or delocalized across the complex as a whole—and this additionally seems to depend on the nature of the metal center and the solvent.[26] Perhaps there exist some disproportionation equilibria amongst the ligands of the reduced complex after subsequent charge transfers, and the complex is re-oxidized at roughly the same onset potential no matter how many ligands are reduced. This hypothesis would be consistent with the observation that the current for reoxidation increases with the number of ligands that were previously reduced. In any case, the $[Fe(bpy)_3](CF_3SO_3)_2$ compound synthesized shows voltammetric behavior in acetonitrile commensurate with other salts of $Fe(bpy)_3^{2+}$ in the literature.

The $CF_3SO_3^-$ salt of $[Fe(bpy)_3]^{2+}$ appears to offer better initial performance in flow-cell cycling than recent attempts using BF_4^-[1,2,4] or FSI.[3] While not immune to performance fade, the system is able to cycle under nontrivial applied current densities and states-of-charge for hundreds of cycles and multiple weeks. After uninterrupted cycling in some capacity for over 11 days at 20 mA cm^{-2}, the system is able to cycle for more than 100 additional cycles at 10 mA cm^{-2}, accessing 50% state-of-charge at just over 80% energy efficiency, demonstrating the promise of this compound for flow-battery applications.

Mechanistic reasons for the discrepancy in longevity between redox-active salts of $Fe(bpy)_3^{2+}$ with different anions were not probed in this work. It is worth highlighting challenges repeatedly observed in nonaqueous flow cells with the BF_4^- salt, however.[1,2,4,6,21] There is still transient performance degradation with the $CF_3SO_3^-$ salt, but the longer lifetime of this system should allow easier deconvolution of the multiple possible background processes. The system's improved longevity compared to literature reports may owe in part to the reduced number of species present in solution, due to the removal of the supporting electrolyte cation.

Active-species degradation may still be present, as a Nernstian end-of-charge vertical asymptote presents itself near the end of the Protocol **IV** cycles, see Fig. 4. It is not clear whether this effect is exacerbated by solvent evaporation and electrolyte imbalance between reservoirs, however. Additionally, the non-monotonic evolution of overpotential, voltaic efficiency, and energy efficiency requires further investigation.

Conventional wisdom suggests that additional supporting electrolyte is necessary in nonaqueous flow batteries to provide solution conductivity. Both here and elsewhere,[1,3] it has been shown that appropriately designed coordination-complex salts can supply sufficient conductivity to unsupported solutions. One of the key advantages of the $[Fe(bpy)_3](CF_3SO_3)_2$ compound is its reasonably high solubility in acetonitrile and its apparently high ionicity relative to other simple salts of the cationic iron complex. The tests presented here were performed using current densities an order of magnitude higher than any used in previous literature, while achieving comparable voltage efficiency, cf. Table I. This higher rate capability suggests that the cell used here has much lower cell resistance, a factor toward which electrolyte conductivity contributes substantially. Of course, other factors beyond the common anion contribute to cell resistance: past work used propylene carbonate rather than acetonitrile and ion-exchange membranes in place of porous separators. Because solutions of similar ionic strengths in acetonitrile tend to be more conductive than their counterparts in propylene carbonate,[36,37] this difference could be important. Finally, it must be observed that cell configurations based on porous separators naturally offer much lower areal resistance than ones with ion-selective membranes.[12,39]

Conclusions

Evidence was presented showing improved nonaqueous flow battery cycling performance for the redox-active $[Fe(bpy)_3]^{2+}$ cation by using $CF_3SO_3^-$ as the anion of the active salt without additional supporting electrolyte. $[Fe(bpy)_3](CF_3SO_3)_2$ was synthesized and characterized with voltammetry, then tested in a flow cell and subjected to different cycling conditions. The cell survived for well over 800 cycles at current densities above 10 mAcm^{-2}, providing substantial improvements (at least 40-fold and 5-fold, respectively) in both cycle life and power capability over literature studies involving similar active species. Performance fade primarily owed

to increasing ohmic loss within the cell as cycling proceeded. Cycling performance presented a number of questions related to transient evolution of cell overpotential and possible active species degradation. The improved longevity and power capability of $[Fe(bpy)_3](CF_3SO_3)_2$ as an active species will make it easier to investigate the class of symmetric common-ion flow-battery systems in further studies. Future research is justified because of the potential benefits offered by a symmetric flow battery based on an iron-centered, supporting-salt-free, high-voltage electrolyte.

Acknowledgments

This work was supported in part by the EPSRC Doctoral Impact Scheme through the University of Oxford's impact acceleration award, grant number EP/R511742/1. KPS and AAW also received support from the Faraday Institution, through subawards FIRG007 and FIRG025 under grant number EP/S003053/1, respectively.

ORCID

Kirk P. Smith https://orcid.org/0000-0003-3412-9948
Rohit Rungta https://orcid.org/0009-0004-1156-7325
Andrew A. Wang https://orcid.org/0000-0003-1864-5213
Charles W. Monroe https://orcid.org/0000-0002-9894-5023

References

1. S. M. Laramie, J. D. Milshtein, T. M. Breault, F. R. Brushett, and L. T. Thompson, "Performance and cost characteristics of multi-electron transfer, common ion exchange non-aqueous redox flow batteries." *Journal of Power Sources*, **327**, 681 (2016).
2. J. D. Milshtein, S. L. Fisher, T. M. Breault, L. T. Thompson, and F. R. Brushett, "Feasibility of a supporting-salt-free nonaqueous redox flow battery utilizing ionic active materials." *ChemSusChem*, **10**, 2080 (2017).
3. T. Blesch, "Studies of an Iron-based, symmetric, non-aqueous redox flow battery." *Ph.D. Thesis*, Monash University (2022), 10.26180/19914244.v1.
4. S. L. Fisher, "Non-aqueous redox flow batteries: active species stability and cost saving design concepts." *Ph.D. Thesis*, The University of Michigan (2017), https://hdl.handle.net/2027.42/140904.
5. J. Mun, D.-J. Oh, M. S. Park, O. Kwon, H.-T. Kim, S. Jeong, Y. G. Kim, and M.-J. Lee, "Highly Soluble Tris(2,2'-bipyridine) Metal Bis(trifluoromethanesulfonyl) imide Complexes for High Energy Organic Redox Flow Batteries." *J. Electrochem. Soc.*, **165**, A215 (2018).
6. C. X. Cammack, H. D. Pratt, L. J. Small, and T. M. Anderson, "A higher voltage Fe (II) bipyridine complex for non-aqueous redox flow batteries." *Dalton Transactions*, **50**, 858 (2021).
7. W. R. McWhinnie and J. D. Miller, "The chemistry of complexes containing 2,2 ′-Bipyridyl, 1, 10-Phenanthroline, or 2,2 ′,6 ′,2"-Terpyridyl as Ligands." *Advances in Inorganic Chemistry and Radiochemistry*, **12**, 135 (1970).
8. M. Chakrabarti, R. Dryfe, and E. Roberts, "Evaluation of electrolytes for redox flow battery applications." *Electrochimica Acta*, **52**, 2189 (2007).
9. N. Tanaka and Y. Sato, "Electrode reactions of tris(2,2'-bipyridine)-iron(II) and tris (2,2 ′-bipyridine)iron(III) complexes in acetonitrile solution." *Electrochimica Acta*, **13**, 335 (1968).
10. W. M. Haynes, D. R. Lide, and T. J. Bruno, *CRC Handbook of Chemistry and Physics: A Ready-Reference Book of Chemical and Physical Data* (Boca Raton, FL) (CRC Press) (2016).
11. D. M. Cabral, P. C. Howlett, and D. R. MacFarlane, "Electrochemistry of the tris (2,2'-bipyridine) complex of iron(II) in ionic liquids and aprotic molecular solvents." *Electrochimica Acta*, **220**, 347 (2016).
12. R. M. Darling, K. G. Gallagher, J. A. Kowalski, S. Ha, and F. R. Brushett, "Pathways to low-cost electrochemical energy storage: a comparison of aqueous and nonaqueous flow batteries." *Energy Environ. Sci.*, **7**, 3459 (2014).
13. W. Ward, "Electrode potential measurements in anhydrous acetonitrile." *Ph.D. Thesis*, The University of Iowa, United States–Iowa (1958), https://proquest.com/docview/301907654?accountid=28541.
14. S. Herzog and R. Taube, "Neutralkomplexe des 2,2'-Dipyridyls Teil I Darstellung und Eigenschaften." *Zeitschrift für Chemie*, **2**, 208 (1962).
15. F. S. Hall and W. L. Reynolds, "Preparation of an Iron(0) Complex with 2,2'-Bipyridine." *Inorg. Chem.*, **5**, 931 (1966).
16. P. Singh, "Application of non-aqueous solvents to batteries." *Journal of Power Sources*, **11**, 135 (1984).
17. M. Morita, Y. Tanaka, K. Tanaka, Y. Matsuda, and T. Matsumura-Inoue, "Electrochemical oxidation of ruthenium and iron complexes at rotating disk electrode in acetonitrile solution." *Bull. Chem. Soc. Jpn.*, **61**, 2711 (1988).
18. Y. Matsuda, K. Tanaka, M. Okada, Y. Takasu, M. Morita, and T. Matsumura-Inoue, "A rechargeable redox battery utilizing ruthenium complexes with non-aqueous organic electrolyte." *Journal of Applied Electrochemistry*, **18**, 909 (1988).
19. J. Mun, M.-J. Lee, J.-W. Park, D.-J. Oh, D.-Y. Lee, and S.-G. Doo, "Non-aqueous redox flow batteries with nickel and iron tris(2,2'-bipyridine) complex electrolyte." *Electrochemical and Solid State Letters*, **15**, A80 (2012).
20. J.-W. Park, M.-J. Lee, S.-S. Hwang, D.-y. Lee, and D.-J. Oh, *REDOX FLOW BATTERY*, U.S. patent number US20120171541A1 (2012).
21. B. D. Silcox, "Stability and cyclability predictions of redox active organic molecules for non-aqueous redox flow batteries." *Ph.D. Thesis*, The University of Michigan (2021), 10.7302/1421.
22. S. Dong, D. M. Cabral, J. M. Pringle, and D. R. Macfarlane, "Exploring the electrochemical properties of mixed ligand Fe(II) complexes as redox couples." *Electrochimica Acta*, **362**, 137109 (2020).
23. L. Meda, F. Oldani, G. Tozzola, S. Caramori, E. Benazzi, V. Cristino, and C. A. Bignozzi, "Searching for new redox-complexes\in organic flow batteries." *Solid State Ionics*, **317**, 142 (2018).
24. E. Benazzi, V. Cristino, S. Caramori, L. Meda, R. Boaretto, and C. A. Bignozzi, "Electrochemical characterization of polypyridine iron(II) and cobalt(II) complexes for organic redox flow batteries." *Polyhedron*, **140**, 99 (2018).
25. R. Chen, "Redox flow batteries: mitigating cross-contamination via bipolar redox-active materials and bipolar membranes." *Current Opinion in Electrochemistry*, **37**, 101188 (2023).
26. C. Creutz, "Bipyridine radical ions." *Comments on Inorganic Chemistry*, **1**, 293 (1982).
27. G. Bontempelli, R. Seeber, S. Zecchin, and G. Schiavon, "Electroanalytical evidences for the instability of hydrogen tetrafluoroborate in acetonitrile." *Journal of Electroanalytical Chemistry and Interfacial Electrochemistry*, **73**, 295 (1976).
28. M. G. Freire, C. M. S. S. Neves, I. M. Marrucho, J. A. P. Coutinho, and A. M. Fernandes, "Hydrolysis of tetrafluoroborate and hexafluorophosphate counter ions in imidazolium-based ionic liquids." *The Journal of Physical Chemistry A*, **114**, 3744 (2010).
29. K. S. Hagen, "Iron(II) triflate salts as convenient substitutes for perchlorate salts: crystal structures of [Fe(H2O)6](CF3SO3)2 and Fe(MeCN)4(CF3SO3)2." *Inorg. Chem.*, **39**, 5867 (2000).
30. G. Inzelt, A. Lewenstam, and F. Scholz, *Handbook of Reference Electrodes* (Berlin, Heidelberg)(Springer Berlin Heidelberg) (2013).
31. R. G. Compton and C. E. Banks, *Understanding Voltammetry* (Europe)(World Scientific) 3rd ed. (2018).
32. K. P. Smith and C. W. Monroe, "Image-based mechanical balancing of reservoir volumes during benchtop flow battery operation." *Frontiers in Chemical Engineering*, **3**, 748865 (2021).
33. K. P. Smith, A. Wang, R. Rungta, and C. Monroe, (2023), Oxford University Research Archive Repository: Cycling and EIS data for Multi-week cycling of a nonaqueous flow battery using tris-bipyridine iron (II) triflate without additional supporting electrolyte https://ora.ox.ac.uk/objects/uuid:58e32eed-829a-4399-a379-2ed879d24d53.
34. A. Wang, "Why has the cost of battery electrolytes halved?" (2023), https://intercalationstation.substack.com/p/why-has-the-cost-of-battery-electrolytes.
35. P. J. Cabrera, X. Yang, J. A. Suttil, R. E. M. Brooner, L. T. Thompson, and M. S. Sanford, "Evaluation of tris-bipyridine chromium complexes for flow battery applications: impact of bipyridine ligand structure on solubility and electrochemistry." *Inorg. Chem.*, **54**, 10214 (2015).
36. K. Izutsu, *Electrochemistry in Nonaqueous Solutions* (Weinheim)(Wiley-VCH) 2nd ed. (2009).
37. D. Aurbach, *Nonaqueous Electrochemistry* (Boca Raton, FL)(CRC Press) (1999).
38. T. Saji and S. Aoyagui, "Electrochemical evidence for aromatic dianion ligands of iron and ruthenium complexes." *Journal of Electroanalytical Chemistry and Interfacial Electrochemistry*, **110**, 329 (1980).
39. R. Darling, K. Gallagher, W. Xie, L. Su, and F. Brushett, "Transport property requirements for flow battery separators." *J. Electrochem. Soc.*, **163**, A5029 (2016).